Journal for ImmunoTherapy of Cancer

T cell-mediated targeted delivery of tadalafil regulates immunosuppression and polyamine metabolism to overcome immune checkpoint blockade resistance in hepatocellular carcinoma

Xiaobin Wang,[1] Qiaoyun Zhang,[2] Jingwen Zhou,[1] Zecong Xiao,[1] Jianxin Liu,[1] Shaohui Deng,[3] Xiaoyang Hong,[1] Wensou Huang,[1] Mingyue Cai,[1] Yongjian Guo,[1] Jingjun Huang,[1] Yong Wang,[2] Liteng Lin,[1] Kangshun Zhu [1]

To cite: Wang X, Zhang Q, Zhou J, *et al*. T cell-mediated targeted delivery of tadalafil regulates immunosuppression and polyamine metabolism to overcome immune checkpoint blockade resistance in hepatocellular carcinoma. *Journal for ImmunoTherapy of Cancer* 2023;**11**:e006493. doi:10.1136/jitc-2022-006493

► Additional supplemental material is published online only. To view, please visit the journal online (http://dx.doi.org/10.1136/jitc-2022-006493).

XW, QZ, JZ and ZX contributed equally.

Accepted 06 February 2023

For numbered affiliations see end of article.

Correspondence to
Professor Kangshun Zhu; zhksh010@163.com

Liteng Lin; linliteng@yeah.net

Yong Wang; wangy488@jnu.edu.cn

ABSTRACT

Background Immune checkpoint blockade (ICB) monotherapy provides poor survival benefit in hepatocellular carcinoma (HCC) due to ICB resistance caused by immunosuppressive tumor microenvironment (TME) and drug discontinuation resulting from immune-related side effects. Thus, novel strategies that can simultaneously reshape immunosuppressive TME and ameliorate side effects are urgently needed.

Methods Both in vitro and orthotopic HCC models were used to explore and demonstrate the new role of a conventional, clinically used drug, tadalafil (TA), in conquering immunosuppressive TME. In detail, the effect of TA on M2 polarization and polyamine metabolism in tumor-associated macrophages (TAMs) and myeloid-derived suppressor cells (MDSCs) was identified. After making clear the aforementioned immune regulatory effect of TA, we introduced a nanomedicine-based strategy of tumor-targeted drug delivery to make better use of TA to reverse immunosuppressive TME and overcome ICB resistance for HCC immunotherapy. A dual pH-sensitive nanodrug simultaneously carrying both TA and programmed cell death receptor 1 antibody (aPD-1) was developed, and its ability for tumor-targeted drug delivery and TME-responsive drug release was evaluated in an orthotopic HCC model. Finally, the immune regulatory effect, antitumor therapeutic effect, as well as side effects of our nanodrug combining both TA and aPD-1 were analyzed.

Results TA exerted a new role in conquering immunosuppressive TME by inhibiting M2 polarization and polyamine metabolism in TAMs and MDSCs. A dual pH-sensitive nanodrug was successfully synthesized to simultaneously carry both TA and aPD-1. On one hand, the nanodrug realized tumor-targeted drug delivery by binding to circulating programmed cell death receptor 1-positive T cells and following their infiltration into tumor. On the other hand, the nanodrug facilitated efficient intratumoral drug release in acidic TME, releasing aPD-1 for ICB and leaving TA-encapsulated nanodrug to dually regulate TAMs and MDSCs. By virtue of the combined application of TA and aPD-1, as well as the efficient tumor-targeted drug delivery, our nanodrug effectively inhibited M2 polarization and polyamine metabolism in TAMs and MDSCs to conquer immunosuppressive TME, which contributed to remarkable ICB therapeutic efficacy with minimal side effects in HCC.

WHAT IS ALREADY KNOWN ON THIS TOPIC

⇒ Immune checkpoint blockade (ICB) monotherapy provides poor survival benefit in hepatocellular carcinoma (HCC) due to ICB resistance and drug discontinuation caused by immune-related side effects. M2-polarized tumor-associated macrophages (TAMs) and myeloid-derived suppressor cells (MDSCs) play a key role in ICB resistance via inducing immunosuppressive tumor microenvironment (TME). As MDSCs can constantly transdifferentiate into M2 TAMs, monotherapy targeting M2 TAMs or MDSCs alone failed to efficiently conquer ICB resistance.

WHAT THIS STUDY ADDS

⇒ Clinically used drug, tadalafil (TA), exerted a new role in dually regulating TAMs and MDSCs by inhibiting M2 polarization and polyamine metabolism in the HCC TME. Aiming at making better use of TA to reverse immunosuppressive TME and overcome ICB resistance for HCC immunotherapy, a dual pH-sensitive nanodrug was successfully developed to facilitate T cell-mediated and tumor-targeted delivery of both TA and programmed cell death receptor 1 antibody. This novel nanodrug achieved remarkable ICB therapeutic efficacy with minimal side effects in HCC.

HOW THIS STUDY MIGHT AFFECT RESEARCH, PRACTICE OR POLICY

⇒ Our study expands the application of TA in reshaping immunosuppressive TME and provides a nanomedicine-based strategy with great potential for breaking the logjam of ICB-based HCC immunotherapy.

Conclusions Our novel tumor-targeted nanodrug expands the application of TA in tumor therapy and holds great potential to break the logjam of ICB-based HCC immunotherapy.

BACKGROUND

Hepatocellular carcinoma (HCC) is the second leading cause of cancer deaths worldwide. Despite the application of multimodal treatments involving surgical resection, local ablation and chemotherapy, the 5-year survival rates of patients with HCC remain extremely low (18%).[1] Recently, immunotherapy, particularly the immune checkpoint blockade (ICB) targeting programmed cell death receptor 1 (PD-1) or programmed death-ligand 1 (PD-L1), has emerged as a promising breakthrough for tumor treatment. However, enthusiasm around anti-PD-1–PD-L1 monotherapy for HCC is now becoming tempered with a relatively low objective response rate (15–20%),[2 3] which may be primarily attributable to ICB resistance caused by the immunosuppressive tumor microenvironment (TME). Besides, adverse events including immune-related pneumonia, hepatitis, myocarditis, and endocrine diseases often occur and lead to drug discontinuation.[4] Thus, novel strategies that can simultaneously overcome ICB resistance and ameliorate side effects are desperately needed for HCC immunotherapy.

Compelling research including our previous study has suggested that tumor-associated myeloid cells, primarily including tumor-associated macrophages (TAMs) and myeloid-derived suppressor cells (MDSCs), induce the immunosuppressive TME to promote tumor progression.[5–7] Macrophages, specialized immune cells involved in the phagocytosis of harmful organisms, possess polarization potentials toward M1 or M2 phenotypes. TAMs more closely resemble the M2-polarized macrophages under the stimulus of various signaling pathways and factors in the TME. It is clear that M2 TAMs impair the T-cell cytotoxicity and promote immunosuppression through secreting immunosuppressive factors (eg, transforming growth factor beta) and chemokines (eg, C–C motif chemokine ligand 2 (CCL2)).[8 9] MDSCs are pathologically activated myeloid cells derived from the myeloid progenitor cells in bone marrow, which not only can produce abundant immunosuppressive factors to impair T-cell cytotoxicity but also can directly transdifferentiate into M2 TAMs to be a constant source for M2 TAMs.[6 10] In addition to the aforementioned immunosuppressive role of M2 TAMs and MDSCs, it is increasingly recognized that dysregulation of polyamine metabolism in M2 TAMs and MDSCs also plays an important role in facilitating immunosuppressive TME.[11] Polyamines, natural metabolites composed of positively charged amines, are essential for both normal and neoplastic cell function.[12] M2 TAMs and MDSCs can overexpress arginase-1 (Arg1) to boost polyamine production by metabolizing arginine.[13] On one hand, polyamine can not only further stimulate the polarization of TAMs toward M2 phenotypes but also activate STAT3 to promote the survival of MDSCs.[14 15] On the other hand, polyamine can upregulate indoleamine 2,3-dioxygenase 1 (IDO1) expression in dendritic cells to induce the apoptosis of T cells.[16] Even worse, polyamine can directly promote the proliferation and survival of tumor cells.[17] Taken together, M2 TAMs and MDSCs promote the immunosuppressive TME and tumor progression directly by means of secreting immunosuppressive factors to impair T-cell cytotoxicity, as well as indirectly dependent on the dysregulated polyamine metabolism. Thus, we speculate that dual regulation of M2 TAMs and MDSCs to reverse the immunosuppressive TME may be a promising strategy against ICB resistance.

Tadalafil (TA), a selective inhibitor of phosphodiesterase type 5 (PDE5), was clinically approved for treating erectile dysfunction and pulmonary hypertension.[18] A recent study reveals that TA can effectively relieve the immunosuppressive effect of MDSCs in HCC by deactivating Arg1.[19] Consistently, our preliminary investigation further discovers that TA can repolarize immunosuppressive M2 macrophages into immune-active M1 ones. Thus, the counteraction of TA on immunosuppressive TME by dually regulating M2 TAMs and MDSCs, as well as the potential of TA as antitumor drug candidate for conquering ICB resistance in HCC, deserves to be explored. Noteworthily, however, expanding the application of TA in tumor therapy via systemic administration may be impeded by its high hydrophobicity, low bioavailability for tumor absorption, and side effects resulting from the indiscriminate inhibition of physiological PDE5.[20 21] Tumor-targeted drug delivery systems based on peripheral circulatory cell-driven nanocarriers have shown great potentials in enhancing the bioavailability of hydrophobic therapeutic agents, improving the therapeutic efficacy and minimizing the side effects.[22]

In the current study, based on that circulating PD-1+ T cells can bind to programmed cell death receptor 1 antibody (aPD-1) and then navigate toward tumor sites by chemotaxis as we previously reported,[23] we developed a TA-encapsulated polymeric micelle decorating with aPD-1 on the surface to bind circulating PD-1+ T cells for tumor-targeted drug delivery. A TME acid cleavable linkage was introduced between aPD-1 and micelle to endow a rapid shedding of antibody in TME, releasing aPD-1 for ICB and leaving residual TA-encapsulated micelle, which can be easily phagocytized by TAMs and MDSCs.[24] After a lysosomal drug release, TA was expected to counteract the immunosuppressive TME by dually regulating M2 TAMs and MDSCs, as well as ameliorating the disordered polyamine metabolism, resulting in an enhanced ICB for HCC immunotherapy combined with aPD-1 (figure 1).

MATERIALS AND METHODS

Reagents

The anti-PD-1 antibody was purchased from Bioxcel Corp (cat# BE0033). The antibodies including anti-CD3 (APC conjugated, cat# 100236), anti-CD4 (PE-Cy7 conjugated, cat# 100422), anti-CD8 (APC-Cy7 conjugated,

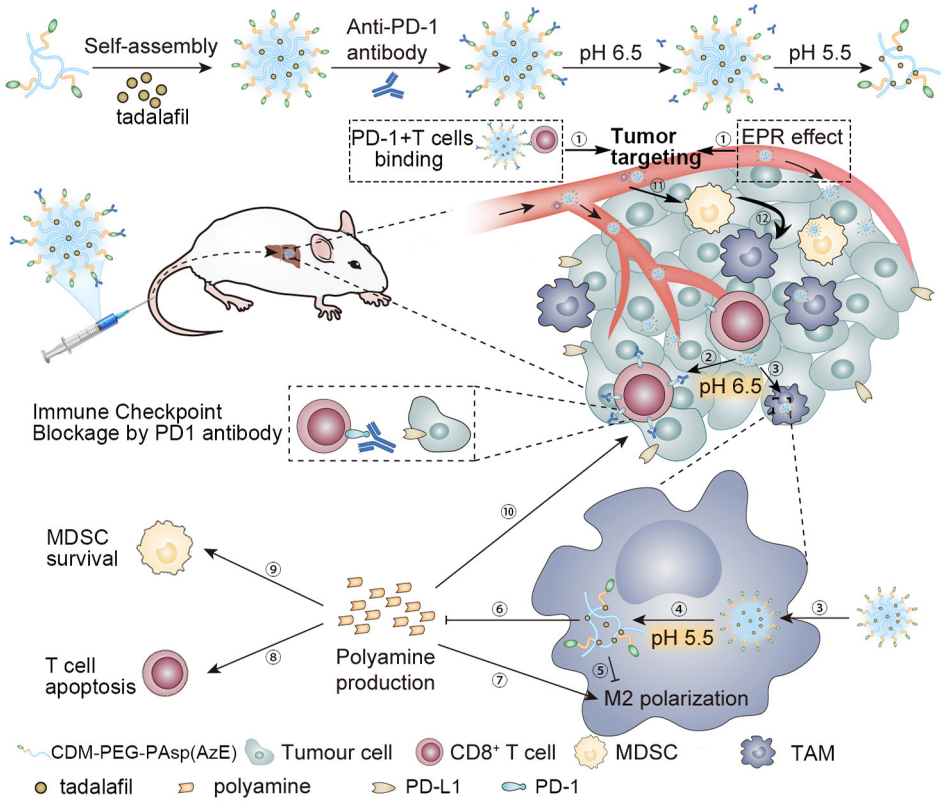

Figure 1 Schematic illustration for the antitumor mechanism of nanodrug in overcoming immune checkpoint blockade resistance in HCC. ① The nanodrug realizes tumor-targeted drug delivery by binding to circulating PD-1+ T cells and following their infiltration into the tumor, as well as by traditional EPR effect. ② The weak acidity (pH ~6.5) of TME triggers first-stage drug release in TME to provide PD-1 antibody for blocking PD-1–PD-L1 axis of cytotoxic T cells. ③–⑥ The first-stage drug release leads to surface charge reversal, leaving a positively charged TA-encapsulated nanodrug which allows an easier drug internalization into TAMs and MDSCs. Then the strong acidity of lysosome triggers a second-stage drug release to provide TA for inhibiting M2 polarization and polyamine production of TAMs and MDSCs to reverse immunosuppressive TME. ⑦–⑩ Nanodrug counteracts the immunosuppressive role of polyamine in stimulating M2 macrophage polarization, promoting MDSC survival, inducing T-cell apoptosis and accelerating tumor proliferation. ⑪ and ⑫ MDSCs can be derived from myeloid progenitor cells in the bone marrow and directly transdifferentiate into M2 TAMs to be a constant source for M2 TAMs. CDM, 2-propionic acid-3-methylmaleic anhydride; EPR, enhanced permeability and retention; HCC, hepatocellular carcinoma; MDSC, myeloid-derived suppressor cell; PD-1, programmed cell death receptor 1; PD-L1, programmed death-ligand 1; TA, tadalafil; TAM, tumor-associated macrophage; TME, tumor microenvironment.

cat# 100714), anti-interferon gamma (IFN-γ) (PE conjugated, cat# 505807), and anti-mouse Foxp3 (Alexa Fluor 488 conjugated, cat# 126405) were purchased from Biolegend for flow cytometry analyses. Alexa Fluor 647-labeled anti-CD8 antibody (cat# 100729) was purchased from Biolegend for immunofluorescence staining. Other antibodies including CD206 (cat# 18704–1-AP), CD80 (cat# 66406–1-Ig), Arg1 (cat# 16001–1-AP), and tubulin (cat# 66031–1-Ig) were purchased from Proteintech (Wuhan, China) for western blotting and immunohistochemical and immunofluorescence staining. Interleukin (IL)-6 antibody (cat# PB0060) was purchased from Boster (Wuhan, China). Foxp3 antibody (cat# 12653) for immunohistochemical staining was purchased from Cell Signaling Technology (Beverly, Massachusetts, USA). α-Allyl-ω-azyl poly(ethylene glycol) (allyl-Polyethylene glycol(PEG)-NH2, Mw=2 kDa), acetic anhydride, 2-mercaptoethanol, 2,2-azobisisobutyronitrile, 2-propionic acid-3-methylmaleic anhydride (CDM), 4-dimethylaminopyridine, anhydrous dimethylformamide, anhydrous dimethyl sulfoxide (DMSO), and acetylacetone manganese were purchased from Sigma-Aldrich. 2-(Azepan-1-yl)ethanamine (AzE) was obtained from J&K Chemical Reagent Co (Beijing, China).

Preparation of nanodrugs

The amphipathic block polymer of CDM-PEG-PAsp(AzE) was first synthesized as described in the online supplemental materials. Subsequently, 20 mg of CDM-PEG-PAsp(AzE) and 2 mg of TA were codissolved into a mixture solution of $CHCl_3$ (1.5 mL) and DMSO (0.5 mL). The resulting solution was emulsified in a 20 mL of phosphate-buffered saline (PBS, pH 7.4) by sonication (VCX130, Sonics, USA; 20 kHz, 30% power level), under the cooling of ice bath. The emulsified solution was evaporated to remove $CHCl_3$, dialyzed against water for 24 hours (Molecular weight cut-off (MWCO): 14 kDa) to remove DMSO, and filtered through a syringe filter

(pore size: 0.22 m) to eliminate large polymer or drug aggregates. The obtained TA loaded micelle was denoted as TA-PPA (CDM-PEG-PAsp(AzE)). For preparation of antibody-decorated nanodrug, the aPD-1 was conjugated to the micellar surface by a reaction of anhydride and primary amine. TA-PPA solution (2 mg/mL) and 350 µL aPD-1 (2.85 mg/mL) were mixed with NHS and EDC as coupling agent at 4°C for 12 hours. Then the nanodrug was ultrafiltrated (MWCO: 300 kDa), washed with fresh PBS for three times to remove excess N-hydroxy succinimide(NHS), 1-ethyl-3-(3-dimethylaminopropyl)carbodiimide hydrochloride(EDC) and free aPD-1, obtaining the aPD-1@TA-PPA. In addition, the blank micelle of PPA, Nile red (NR) loaded micelle of aPD-1@NR-PPA, and DiR loaded micelle of aPD-1@DiR-PPA, were prepared by using the aforementioned method.

In vitro drug release

The in vitro drug release profile of TA from aPD-1@TA-PPA was determined at different pH values using the dialysis method. Briefly, a dialysis bag (MWCO, 14 kDa) containing 3 mL of aPD-1@TA-PPA solution was placed in 30 mL of release medium at different pH values (pH 7.4, 6.5, and 5.0) in a constant temperature shaker (37°C at 100 rpm). At predetermined time intervals, 3 mL of solution outside the dialysis bag was collected and replaced with an equal volume of the same fresh medium. The concentration of TA was measured using Ultraviolet–visible spectroscopy (UV-vis), and the in vitro release experiments were performed in triplicate.

T-cell binding in vitro

T cells were isolated from the spleen of C57BL/6 mice bearing tumor by commercial kit (Miltenyi Biotec, Germany). T cells were cultured in Roswell Park Memorial Institute (RPMI) 1640 medium (Gibco, USA) supplemented with 10% Fetal bovine serum (FBS) at a density of 1×10^7 cells/mL. T cells were incubated with aPD-1@NR-PPA at different times (12 and 24 hours) at pH 7.4 to allow binding. To further evaluate the detachment of nanodrug from T cells, the medium pH was adjusted to pH 6.5; the T cells were incubated at different times (12 and 24 hours) at pH 6.5 to allow detachment. The T cells were stained with Alexa Fluor 647 anti-mouse CD8 antibody and secondary antibody Alexa Fluor 488 for aPD-1 for 1 hour, while the nuclei were stained with Hoechst 33 342 for 15 min. Finally, the cell images were captured by Confocal laser scanning microscopy (CLSM) (Zeiss LSM880, Germany).

Cellular uptake of the nanodrug

Primary macrophages were isolated from the femurs of C57BL/6 mice bearing tumor and stimulated by 20 nM macrophage colony-stimulating factor (M-CSF). The macrophages were further stimulated by 25 nM IL-4 to induce M2 polarization. MDSCs were isolated from the spleen of C57BL/6 mice bearing tumor by commercial kit (Miltenyi Biotec). M2 macrophages or MDSCs were seeded in 35 mm confocal dishes at a density of 1×10^4 cells per well and were cultured overnight, followed by incubation with aPD-1@NR-PPA at pH 7.4 or pH 6.5 for 4 hours. For CLSM observation, the cells were fixed by 4% paraformaldehyde and stained by 4′,6-diamidino-2-phenylindole for cell nucleus location. For flow cytometry analyses, M2 macrophages or MDSCs were seeded in 12-well plates at a density of 1×10^6 cells per well and were cultured overnight, followed by incubation with aPD-1@NR-PPA at pH 7.4 or 6.5 for 1, 2 and 4 hours. Then, the cells were collected and resuspended in PBS and analyzed by Attune NxT Acoustic Focusing Cytometer (Thermo Fisher Scientific, USA). The data were analyzed using FlowJo V.10.0.

HCC animal model and treatment

The orthotopic HCC model was established in male C57BL/6 mice (age: 6 weeks, weight: about 20 g) as we previously described.[5] Briefly, after performing midline incision of the mouse abdomen, 1×10^6 matrigel-mixed Hep1-6 cells (possessing cell line authentication) were injected into the liver followed by placing Gelfoam into the needle track. Finally, the muscle and skin layers of the abdominal wall were then well closed. Then HCC mice were divided into different groups according to randomization principle: PBS, free TA, TA-PPA, aPD-1@PPA, or aPD-1@TA-PPA. Free TA was administrated through intraperitoneal injection, while other drugs are administrated through tail vein injection. The aPD-1 and TA doses per injection, if applied, were 1.2 and 2 mg/kg, respectively.

T cell-binding assay in vivo

HCC mice were injected via tail vein with aPD-1@NR-PPA. The blood of mice was collected at different time points (0, 12, and 24 hours) and blood T cells were purified using Ficoll-Hypaque solution (MP Biomedicals, USA). The T cells were incubated by CD8 antibody and stained by Hoechst 33342, respectively. Then the T cells were observed by CLSM. To evaluate the aPD-1-blocked CD8+ T cells in the tumor site, we isolated the tumor-infiltrated T cells by a commercial T-cell isolation kit. The tumor-infiltrated T cells were stained with anti-CD8 antibody and secondary antibody IgG-APC-Cy7 (aPD-1) for 1 hour. Then, the cells were washed and analyzed by Attune NxT Acoustic Focusing Cytometer (Thermo Fisher Scientific), and the data were analyzed by FlowJo V.10.0 (Treestar, USA).

MRI scan in vivo

Before the beginning of treatment and on days 7 and 14 after the first treatment, MRI scans were performed to evaluate the growth of tumors in the orthotopic HCC mice. Orthotopic tumors were detected by MRI (Intera; Philips Medical Systems, Best, Netherlands) with a clinical 3.0 T system as we previously described.[5] Tumor volume was calculated as follows: tumor volume=$0.5\times\text{length}\times\text{width}^2$.

Statistics

All data were expressed as means±SD. Statistical differences between two groups were analyzed by unpaired

Student's t-test, and differences between multiple groups were analyzed by one-way analysis of variance with Bonferroni correction (GraphPad Prism V.8.0). A p value of <0.05 was considered statistically significant.

RESULTS

TA suppressed M2 macrophage polarization

M2 TAMs and MDSCs are known to play a central role in initiating and perpetuating immunosuppression, which mediated the pathogenesis of various tumors including HCC.[5–7] Though the inhibitory effect of TA on the immunosuppressive function and intratumoral accumulation of MDSCs has been recently revealed in HCC,[19] its influence on M2 TAMs remains unclear. Herein, IL-4-stimulated macrophages were used as a classical M2-TAM model. We explored whether TA could modulate M2 polarization in IL-4-stimulated Raw264.7 macrophage cell line and primary macrophages isolated from mice femur bones. As shown in figure 2A–E, immunofluorescence, quantitative real-time PCR, western blotting and flow cytometry results consistently showed that TA significantly suppressed M2 polarization (Arg1, CD206, and IL-6 as markers) and promoted M1 polarization (CD80, inducible nitric oxide synthase (iNOS), tumour necrosis factor alpha (TNF-α) as markers) in macrophages. It has been recently demonstrated that the overexpressed Arg1 in M2 TAMs metabolizes arginine to produce abundant polyamine to mediate immunosuppression and stimulate tumor proliferation.[14 17] We next evaluated whether the downregulated Arg1 by TA could decrease the polyamine production. According to the ELISA results, TA markedly reduced the generation of polyamine in M2 macrophages (figure 2C).

Growing evidence are suggesting that M2 TAMs blunt the efficacy of anti-PD-1–PD-L1 therapy in multiple tumors via diverse mechanisms.[25 26] As shown in figure 2B, compared with TA or aPD-1 monotherapy, the combination therapy of TA and aPD-1 exerted the most potent inhibition on M2 macrophage polarization. Meanwhile, the least polyamine production was also observed in M2 macrophages receiving the combination therapy (figure 2C). Taken together, these in vitro results indicated that the effective regulation on M2 macrophages and Arg1/polyamine metabolism by combination therapy of TA and aPD-1 may serve as a synergistic mechanism for improved immunotherapy.

TA reactivated CD8+ T cells by dually regulating TAMs and MDSCs

M2 TAMs and MDSCs can overexpress Arg1 to boost the production of polyamine, which has been well demonstrated to directly stimulate the proliferation and survival of tumor cells, and also to serve as a crucial immunosuppressive factor to inactivate CD8+ T cells, the key executors for tumor-specific cytotoxicity.[14–17] As we have shown that TA can suppress M2 macrophage polarization while downregulating the production of polyamine, we next investigated the impact of TA-treated M2-TAMs/MDSCs on T-cell activation and tumor growth. The coculture system of splenic CD8+ T cells isolated from immunocompetent mice, MDSCs/M2 macrophages and Hep1-6 HCC cells was established as previously described.[19 27] IFN-γ, a classical cytokine that supports CD8+ T-cell differentiation and initiates antitumor immunity together with cytotoxic cytokines (eg, granzyme B and perforin), has been well identified as a key marker of the activation and tumor-killing ability of T cells.[28] The flow cytometry and ELISA analyses, respectively, revealed that TA pretreatment for M2-TAMs/MDSCs significantly increased the IFN-γ+ proportion and IFN-γ secretion of CD8+ T cells in the coculture system (figure 2G–J). Then, we further evaluated the antitumor cytotoxic effect of CD8+ T cells by CCK-8 and lactate dehydrogenase assay. As shown in figure 2K,L, the MDSCs or M2-TAMs severely blunted the tumor cytotoxic activity of CD8+ T cells, and such an effect could be efficiently abolished by TA treatment. Therefore, we demonstrated that TA could rescue the antitumor cytotoxic effect of CD8+ T cells suppressed by M2 TAMs and MDSCs.

Synthesis and characterization of pH-sensitive copolymer and nanodrug

The polymer was synthesized via multisteps as shown in online supplemental scheme S1 and the successful synthesis of polymer was verified by proton nuclear magnetic resonance (^{1}H NMR) and Fourier transform infrared (FTIR) analysis. α-Allyl poly(ethylene glycol)-b-poly (β-benzyl L-aspar-tate), namely, allyl-PEG-PBLA, was first synthesized by a ring opening polymerization of BLA-NCA using the allyl-PEG-NH_2 as an initiator. As shown in online supplemental figures S1,2, the characteristic peaks of benzyl-aspartate units (7.28, 5.03, 4.60, and 2.51~2.92 ppm) and methylene of initiator (3.52 ppm) were clearly shown, indicating the successful synthesis. The average degree of polymerization for PBLA was calculated to be 32, by comparing the characteristic chemical shift integral of the benzyl group (7.28 ppm) and the methylene group (3.52 ppm) in the ^{1}H NMR spectra. Then, 2-mercaptoethanol was reacted with the allyl group by Michael addition reaction, showing the disappearance of characteristic peaks for allyl double bond (5.54-5.60 ppm) meanwhile the appearance of characteristic peak for 2-mercaptoethanol (3.33 ppm) by ^{1}H NMR analysis (online supplemental figure S3). Subsequently, HO-PEG-PAsp(AzE) was synthesized by aminolysis of HO-PEG-PBLA(poly-beta-benzyl-L-aspartate) with 2-(azepan-1-yl) ethanamine (AzE) as reported.[29] After the aminolysis, the characteristic peaks of benzyl groups (7.28 ppm) disappeared whereas the characteristic peaks of methylene groups of AzE appeared (1.66, 3.09 ppm) (online supplemental figure S4). The completed aminolysis was also verified by FTIR analysis (online supplemental figure S5), showing the disappearance of characteristic vibration absorption peaks for benzyl ester in PBLA at 1730 cm^{-1} ($\nu_{C=O}$, ester), 745 cm^{-1} and 696 cm^{-1} (δ_{Ph-H}). Finally,

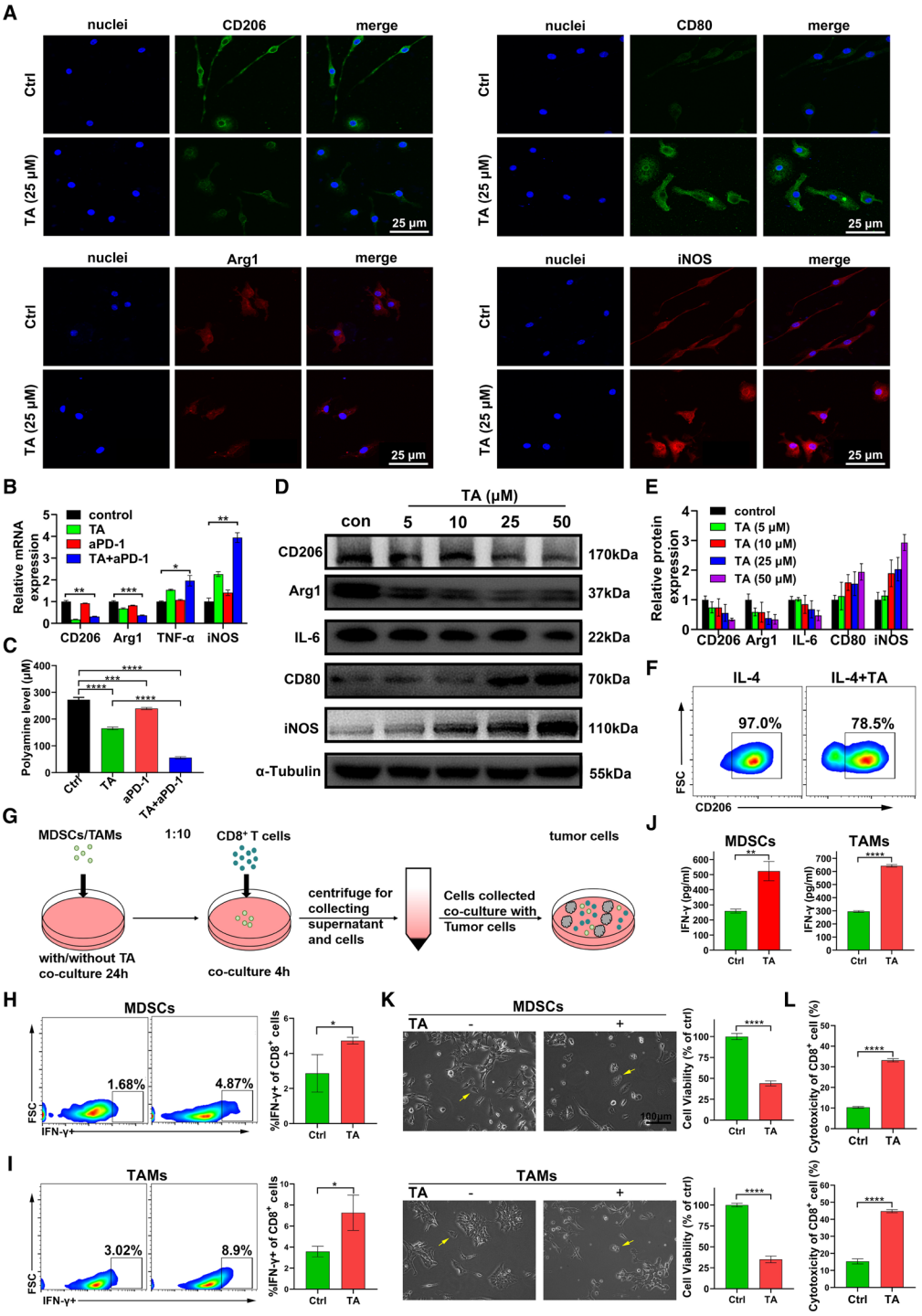

Figure 2 TA significantly suppressed M2 polarization of macrophages in vitro. (A) Morphological transformation and representative immunofluorescent staining of M1 markers (CD80 and iNOS) and M2 markers (CD206 and Arg1) in M2 macrophages treated with 25 μM TA for 48 hours. (B) The mRNA levels of CD206, Arg1, TNF-α, and iNOS in M2 macrophages were measured by qRT-PCR. n=3. (C) The secretion levels of polyamine were measured by ELISA (n=3). (D,E) Protein expression levels of CD206, iNOS, CD80, Arg1, and IL-6 in M2 macrophages treated with different concentrations of TA were determined by western blot. (F) CD206+ macrophages (gated on CD11b+F4/80+ macrophages) were quantitatively determined by flow cytometry assay. (G) Schematic illustration of coculture system. (H,I) IFN-γ+CD8+ T cells in the coculture system were quantitatively determined by flow cytometry assay. (J) The secretion levels of IFN-γ were measured by ELISA (n=3). (K) Morphological changes and viability of Hep1-6 HCC cells in coculture system with or without TA treatment. Hep1-6 cell viability was evaluated by CCK-8 assays (n=3). (L) T-cell cytotoxicity to tumor cells was evaluated by LDH assay (n=3). *P<0.05, **P<0.01, ***P<0.001, ****P<0.0001. aPD-1, programmed cell death receptor 1 antibody; Arg1, arginase-1; Ctrl, control; HCC, hepatocellular carcinoma; IFN-γ, interferon gamma; IL, interleukin; LDH, lactate dehydrogenase; MDSC, myeloid-derived suppressor cell; RT-qPCR, real-time quantitative polymerase chain reaction ; TA, tadalafil; TAM, tumor-associated macrophage; TNF-α, tumour necrosis factor alpha; FSC, forward scatter.

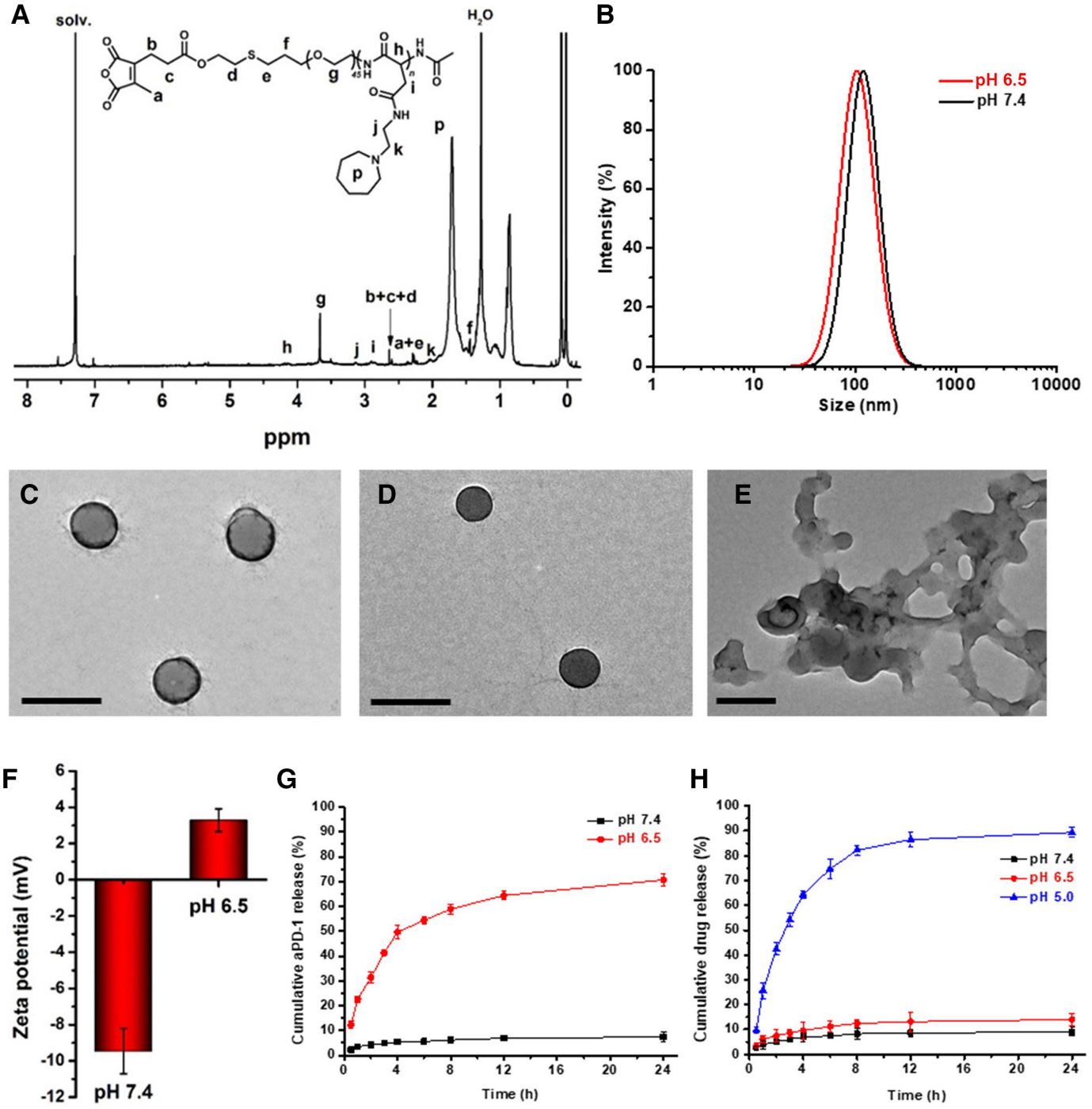

Figure 3 Characterizations of polymer and nanodrug. (A) ^{1}H NMR spectrum of CDM-PEG-PAsp(AzE) in $CDCl_3$. (B) The particle sizes of nanodrug at pH 7.4 and pH 6.5 determined by DLS (n=3, mean±SD). (C–E) TEM images of nanodrug at various pH values of 7.4, 6.5, and 5.0, respectively. Scale bar=200 nm. (F) The zeta potentials of nanodrug at pH 7.4 and pH 6.5 determined by DLS (n=3, mean±SD). (G) In vitro aPD-1 release from nanodrug at pH 7.4 and pH 6.5 (n=3, mean±SD). (H) In vitro drug release from nanodrug at pH 7.4, pH 6.5, and pH 5.0, respectively (n=3, mean±SD). aPD-1, programmed cell death receptor 1 antibody; CDM, 2-propionic acid-3-methylmaleic anhydride; DLS, dynamic light scattering; TEM, Transmission electron microscopy.

2-propionic acid-3-methyl maleic anhydride (CDM) was conjugated to the polymer, which resulted in a characteristic peak (2.13 ppm) in the ^{1}H NMR spectra of CDM-PEG-PAsp(AzE) (figure 3A).

The pH-sensitive copolymer was self-assembled into a micelle with TA encapsulated in the hydrophobic core (TA-PPA). Then aPD-1 was conjugated to the surface of as-prepared micelle to obtain final nanodrug (aPD-1@TA-PPA). The loading content of TA and aPD-1 were 6.4±0.4% and 3.5±0.3%, as detected by UV-vis and ELISA, respectively. Measurement with dynamic light scattering (DLS) analysis (figure 3B) showed that the particle sizes

of aPD-1@TA-PPA was 120.5±8.7 nm and 102.1±7.4 at pH 7.4 and 6.5. The decreased particles size of nanodrug at pH 6.5 might be attributed to the release of aPD-1. As demonstrated by TEM observation, aPD-1@TA-PPA exhibited a spherical morphology around 100 nm at pH 7.4 (figure 3C), which was in line with the results of DLS detection. Additionally, a darker aPD-1 layer on the nanodrug surface was clearly observed, since the antibody is much easier to be stained with uranyl acetate.[30] When the pH value changed to 6.5, the nanoparticles became smaller; meanwhile, the aPD-1 layer disappeared (figure 3D), implying the antibody was shed from nanodrug. More pieces of evidence were obtained from the in vitro aPD-1 release assay, finding nearly 60% aPD-1 was released from nanodrug at pH 6.5 within 4 hours (figure 3G). The results demonstrated that the antibody could be efficiently released responded to TME acidity, which was essential for aPD-1 to activate the cytotoxic T cells. Moreover, the aPD-1 release induced a potential reversal of nanodrug from −9.5±1.3 mV to+3.3 ± 0.6 mV (figure 3F), owing to the shedding of negatively charged antibody and the protonation of AzE groups,[31] which might facilitate the endocytosis of nanodrug by TAMs and MDSCs. The in vitro release profiles of TA from aPD-1@TA-PPA at different pH values were shown in figure 3H. At both pH of 7.4 and pH 6.5 mimicking the blood environment and tumor tissue acidity, respectively, less than 15% TA was released in 24 hours. When the pH value was changed to 5.0, the 24 hour cumulative release of TA increased to 80%, implying a quick drug release could be triggered in the lysosomal compartments (pH 5.0) of TAMs and MDSCs. Based on these results, the nanodrug was capable of sequentially release aPD-1 in tumor tissue and TA inside targeted cells by responding to the TME and lysosomal acidity, respectively.

To evaluate the serum stability of nanodrug, we detected the particle size of aPD-1@TA-PPA in serum condition against time, and non-significant size change was detected over the experimental time range (online supplemental figure S6a), which implied that our nanodrug was stable in serum. Additionally, the cytotoxicities of nanodrug (aPD-1@TA-PPA, figure 4) were evaluated by CCK-8 assay. As shown in online supplemental figure S6b, Hep1-6 cells, RAW264.7 cells, and LO2 cells (human hepatocytes) incubated with aPD-1@TA-PPA exhibited almost no decrease in viabilities at working concentration, indicating low cytotoxicity of the nanodrug.

In vitro T-cell binding and cellular uptake of nanodrug

Based on making clear the counteraction of TA against the immunosuppressive effect of M2-TAMs and MDSCs as described previously, it is reasonable to assume that TA may serve as an antitumor drug candidate for conquering ICB resistance in HCC by regulating immunosuppressive TME. However, we also notice that TA shows a poor bioavailability in the tumor tissue, as well as unfavorable side effects due to non-specific inhibition of the physiological PDE5,[20 21] which may collectively lead to limited antitumor effect of TA monotherapy[32 33] and impede its clinical antitumor translations. Aiming at resolving the aforementioned issues, we developed a peripheral circulatory T cell-driven nanocarrier with dual-pH sensitivities to facilitate tumor-targeted delivery of TA and aPD-1.

CD8+ T cells (purple Alexa Fluor 647) were selected as a target in the in vitro binding study in order to show the activation of nanodrug on antitumor immunity via effectively binding to CD8+ T cells. At pH 7.4 mimicking the physiological circulating environment, the fluorescence signals of both aPD-1 (green Alexa Fluor 488) and TA (represented by hydrophobic red fluorescence of NR) gradually increased as incubation time went on and were mainly located on the surface of CD8+ T cells (figure 4A), which indicated the successful binding of nanodrug to CD8+ T cells dependent on the PD-1–aPD-1 interaction rather than cellular internalization. At pH 6.5 mimicking the tumor extracellular microenvironment, the red fluorescence signals on cell surface rapidly weakened as incubation time went on, which indicated the separation of the NR-labeled micelle from CD8+ T cells via CDM linkage cleavage under slightly acidic environments. The aforementioned in vitro results laid a foundation for the potential of our CD8+ T cell-binding nanodrug not only to realize tumor-targeted drug delivery accompanied with the intratumoral infiltration of CD8+ T cells, but also to facilitate first-stage drug release in response to the acidic TME (pH 6.5), providing aPD-1 to block PD-1 of T cells and leaving a positively charged TA-PPA to dually regulate MDSCs and M2 macrophages.

Next, MDSCs and M2 macrophages were selected as the TA target cells for the in vitro drug uptake study. As evidenced by CLSM observation, both MDSCs and M2 macrophages showed obvious NR red fluorescence in the cytoplasm after 4 hours incubation at pH 6.5, which indicated the efficient cellular internalization of nanodrug. By contrast, cells incubated at pH 7.4 showed little drug uptake (figure 4B,C). The aforementioned results were also quantitatively confirmed by flow cytometry analyses (figure 4D). These results indicated that TA-PPA could be readily taken up by MDSCs and M2 macrophages, which could be attributed to the surface charge conversion from negative to positive after the first-stage aPD-1 release, as well as to the high endocytic capacities of MDSCs and macrophages.[24]

Tumor accumulation and biodistribution in vivo

In vivo binding of the nanodrug to CD8+PD-1+ T cells was investigated. Twelve hours after aPD-1@NR-PPA was injected into mice via tail vein, the blood T cells were isolated and observed by CLSM. As shown in figure 4E, most CD8+ T cells (green Alexa Fluor 488) were decorated with red fluorescent NR (red arrow), indicating an effective binding of aPD-1@NR-PPA to CD8+ T cells. Moreover, 24 hours after the injection of aPD-1@TA-PPA, the tumor-infiltrating T cells were also isolated for quantitative flow cytometry analysis. As shown in figure 4F, only 17.1% of the tumor-infiltrating CD8+ T cells in the

Figure 4

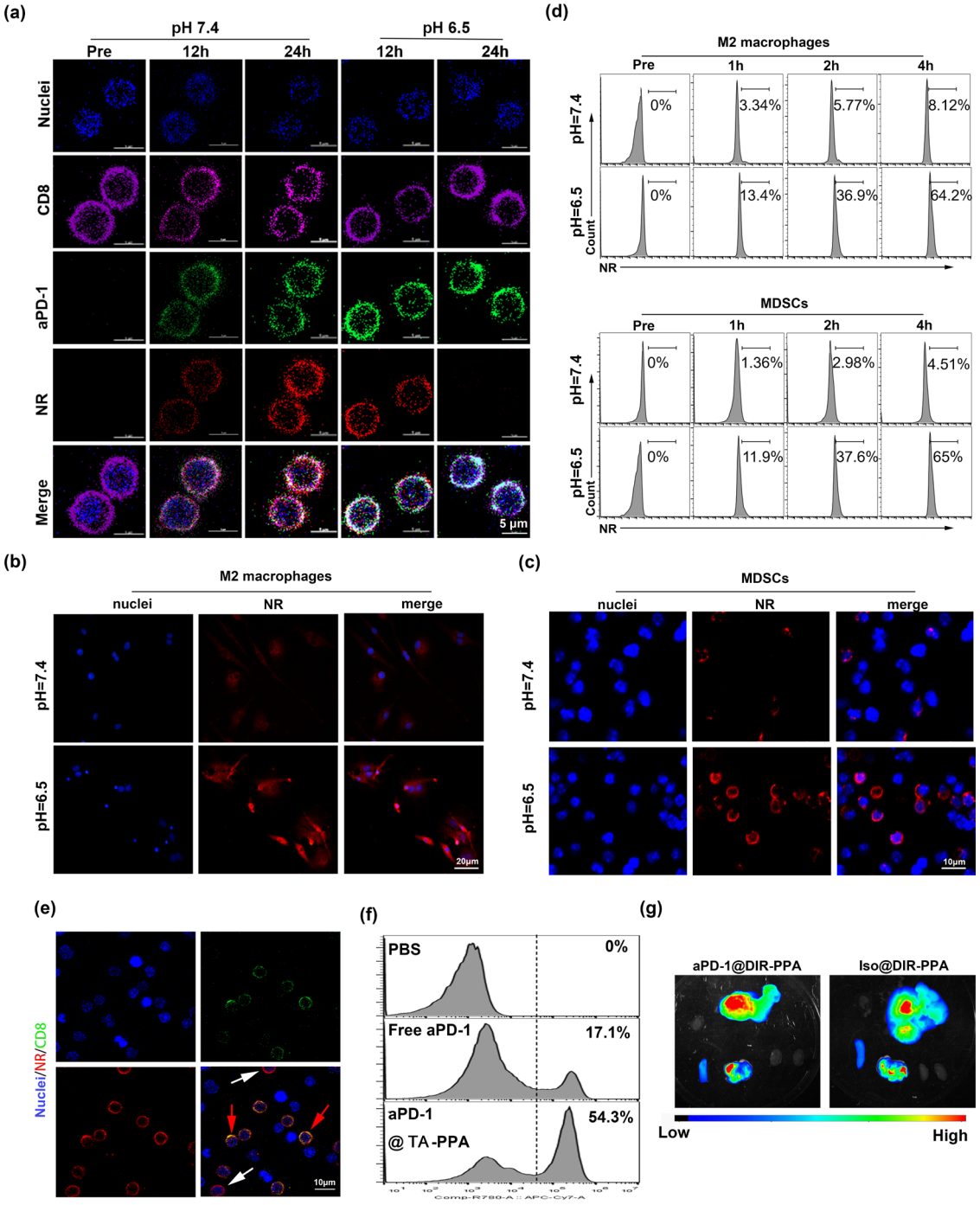

Figure 4 T cell-mediated drug delivery in vitro and in vivo. (A) CD8+ T cells (purple Alexa Fluor 647) were selected as a target in the in vitro binding study. aPD-1 was labeled with green Alexa Fluor 488, and TA was represented by hydrophobic red fluorochrome NR for fluorescence visualization. The binding of aPD-1@NR-PPA to PD-1+ T cells at pH 7.4 or 6.5 was revealed by CLSM imaging. (B–D) Cellular uptake of aPD-1@NR-PPA in M2 macrophages and MDSCs at pH 7.4 or 6.5 was determined by CLSM imaging and flow cytometry, respectively. (E) All blood lymphocytes were isolated at 12 hours after tail vein injection. CLSM images showed the binding of aPD-1@NR-PPA to CD8+ T cells. CD8+ T cells were labeled by green Alexa Fluor 488 fluorescence, and TA was replaced by red fluorescence NR for fluorescence visualization. Red arrows show the nanodrug-bound PD-1+CD8+ T cells, and white arrows show PD-1+CD8– T cells attached with nanodrug. (F) The proportion of tumor-infiltrating CD8+ T cells blocked by APC-Cy7-labled aPD-1 was analyzed by flow cytometry. (G) Representative fluorescence imaging of the hepatic tumor and main organs harvested from mice bearing orthotopic HCC at 24 hours after intravenous injection of Iso@DiR-PPA or aPD-1@DiR-PPA. The near-infrared fluorescent dye DiR instead of TA was loaded into the nanocarrier for fluorescence imaging in vivo. aPD-1, programmed cell death receptor 1 antibody; DiR, 1,1′-dioctadecyl-3,3,3′,3′-tetramethylindotricarbocyanine iodide; HCC, hepatocellular carcinoma; MDSC, myeloid-derived suppressor cell; NR, Nile red; PBS, phosphate-buffered saline; PD-1, programmed cell death receptor 1; TA, tadalafil

mice receiving free aPD-1 were blocked by aPD-1 (APC-Cy7 positive), while the APC-Cy7-positive cells were raised to 54.3% when the mice were treated by aPD-1@TA-PPA. This result indicated that our drug delivery strategy effectively blocked the PD-1–PD-L1 axis.

Next, in vivo fluorescence imaging was performed to further evaluate the nanodrug biodistribution after injection into mice via tail vein. The near-infrared fluorescent dye 1,1′-dioctadecyl-3,3,3′,3′-tetramethylindotricarbocyanine iodide (DiR) instead of TA was loaded into the micelle for fluorescence imaging in vivo. As shown in figure 4G, both Iso@DiR-PPA and aPD-1@DiR-PPA displayed significant hepatic accumulation at 24 hours after intravenous injection probably due to the entrapment by the hepatic reticuloendothelial system.[34] Notably, compared with the Iso@DiR-PPA group, the aPD-1@DiR-PPA group showed more intensive DiR fluorescence in the hepatic tumor area. Thus, as evidenced by the in vivo fluorescence imaging, aPD-1-decorated micelle possessed favorable tumor-targeting ability for drug delivery in mice bearing orthotopic HCC.

TA reversed the immunosuppressive TME by regulating M2 TAMs and MDSCs

Tumor growth is a complex process affected by the mutual interaction between multiple immune cells in the TME. In particular, infiltrating CD8+ T cells play a key antitumor role by tumor-specific cytotoxicity, whereas M2 TAMs, MDSCs and regulatory T cells (Tregs) behave as main immunosuppressive cells which cause tumor immune escape.[35] In addition to making clear the inhibitory effect of TA on M2 macrophage polarization in vitro (figure 2), our in vivo data of flow cytometry determined that TA was also capable of suppressing M2 polarization of TAMs and reducing the proportion of MDSCs (CD11b+Gr+) in mice bearing orthotopic HCC (figure 5A,B). Meanwhile, TA administration significantly reduced the polyamine production in the HCC tumor tissues (figure 5). Based on the aforementioned findings confirming the effective inhibition of TA on M2 TAMs, MDSCs and polyamine production in tumor tissues, we further found that TA administration significantly decreased the proportion of Treg cells (CD4+Foxp3+) (figure 5C,D). Interestingly, CL2, a classical chemokine which is mainly produced by both tumor cells and myeloid cells and plays a crucial role in promoting the recruitment of immunosuppressive cells (eg, MDSCs and Treg cells),[36] was significantly reduced in the tumor tissues of the TA-treated group as indicated by the ELISA results (figure 5G). Although the underlying mechanism mediating such an effect of TA remains to be further identified, it suggested that CCL2

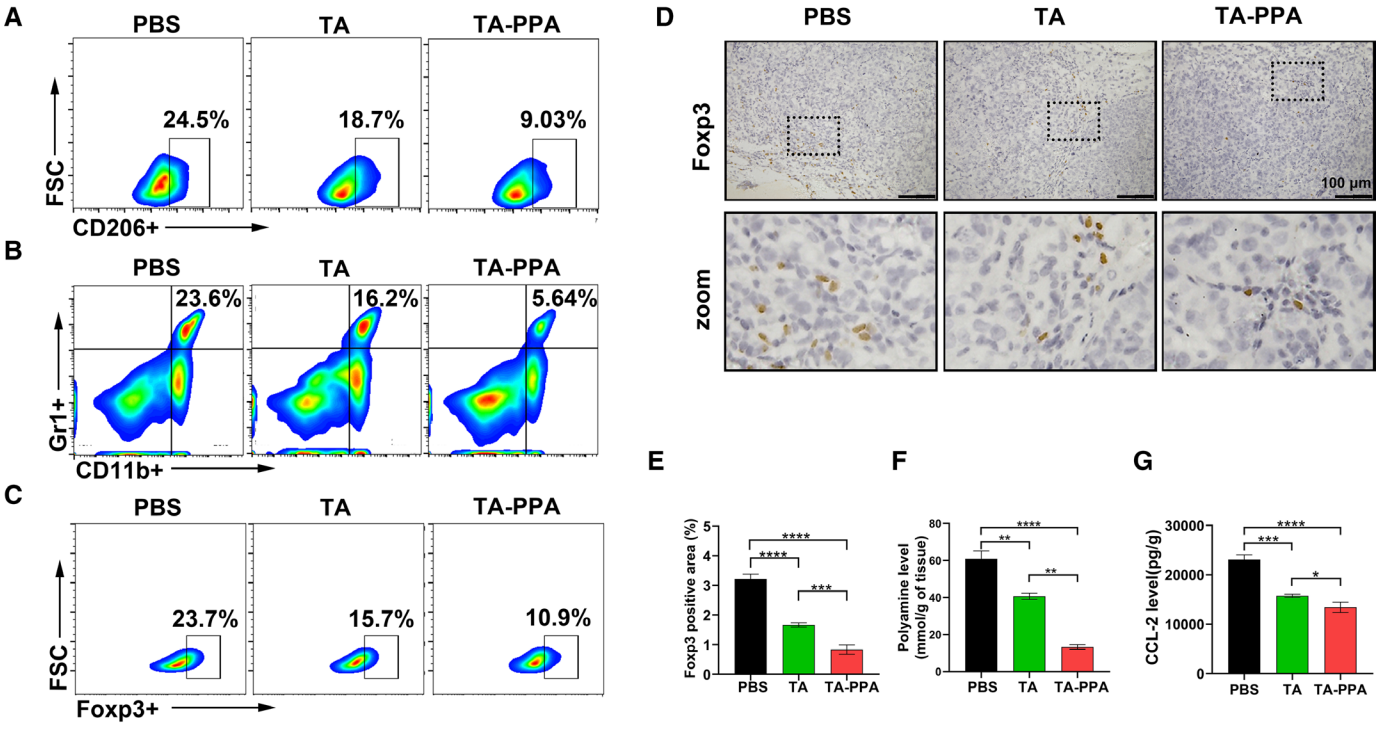

Figure 5 TA regulated M2 TAMs and MDSCs to reverse the immunosuppressive TME. (A–C) M2 macrophages (CD206+, gated on CD11b+F4/80+ cells), MDSCs (Gr1+, gated on CD11b+ cells) and Treg cells (Foxp3+, gated on CD3+CD4+ cells) in Hep1-6 tumor tissues were quantitatively determined by flow cytometry assay. (D,E) Representative immunohistochemical staining showed Treg cells (Foxp3+, brown) in Hep1-6 tumor tissues. (F) Expression levels of polyamine in Hep1-6 tumor tissues were analyzed by ELISA assay. n=3. (G) Expression levels of immunosuppressive chemokine CCL2 in Hep1-6 tumor tissues were analyzed by ELISA assay (n=3). *P<0.05, **P<0.01, ***P<0.001, ****P<0.0001. CCL2, C–C motif chemokine ligand 2; MDSC, myeloid-derived suppressor cell; PBS, phosphate-buffered saline; TA, tadalafil; TAM, tumor-associated macrophage; TME, tumor microenvironment.

might be a vital mediator involved in the regulation of TA on the immunosuppressive TME. Moreover, the aforementioned counteraction of TA administration against the immunosuppressive TME was significantly strengthened in the group receiving TA-PPA (figure 5A–E), which could be attributed to the enhanced cell uptake of nanodrug facilitated by the TME acidity and also to the lysosomal acidity-triggered intracellular TA release. Taken together, TA delivered by nanocarrier displayed a great in vivo performance to counteract the immunosuppressive TME of HCC by simultaneously regulating M2 TAMs and MDSCs, which pushed forward our next investigation on the previously unknown role of TA in conquering ICB resistance for HCC treatment.

Nanodrug regulated TME and achieved enhanced therapeutic outcome in HCC

To verify the role of TA in conquering ICB resistance for HCC treatment, mice bearing orthotopic HCC were administrated by different therapies (TA-PPA, aPD-1-PPA, or the combination of TA and aPD-1, ie, aPD-1@TA-PPA) via tail vein injection. We appraised the effect of combination therapy of TA and aPD-1 on the HCC immune microenvironment by flow cytometry and immunohistological analyses. As expected, the group receiving aPD-1-PPA alone displayed a slightly increased proportion of M1 TAMs (CD80, iNOS as marker) and CD8+ T cells, and a mildly reduced proportion of M2 TAMs (Arg1, CD206 as marker), Tregs and MDSCs in the tumor tissues (figure 6A–D), which was consistent with previous reports demonstrating the promotion of aPD-1 on antitumor immunity.[37] Inspiringly, the combination therapy of aPD-1@TA-PPA showed the most effective modulation on HCC immune microenvironment as evidenced by the highest proportion of M1 TAMs and CD8+ T cells, and the lowest proportion of M2 TAMs, Tregs and MDSCs in the tumor tissues (figure 6A–D). In addition, the highest INF-γ level were also confirmed in the aPD-1@TA-PPA group (figure 6E). These in vivo results verified that codelivery of TA and aPD-1 jointly fostered an antitumor immune microenvironment.

Next, the antitumor effect of different therapies was further evaluated. On one hand, compared with the monotherapy of TA-PPA or aPD-1-PPA, the combination therapy of aPD-1@TA-PPA exhibited the most potent suppression on tumor growth as determined by the MRI scan and anatomical observation, and brought the longest survival for the animals until the end point of observation (figure 7A–E). Consistent with the aforementioned findings, the combination antitumor effect of TA and aPD-1 was histologically confirmed by terminal deoxynucleotidyl transferase-mediated dUTP-biotin nick end labeling (TUNEL) assay, which showed the highest level of tumor necrosis in the group receiving aPD-1@TA-PPA (figure 7F,G). On the other hand, compared with other groups, only the combination therapy by aPD-1@TA-PPA showed an effective prevention on lung metastasis in the mice bearing orthotopic HCC (figure 7H). Furthermore, according to the in vivo MRI imaging and general view of orthotopic HCC, the group of aPD-1@TA-PPA nanodrug possessed a significantly better curative effect against HCC in comparison to the free drugs (free TA+ free aPD-1) group (online supplemental figure S7).

Side effects in vivo

As shown in figure 7E,H staining showed that aPD-1@TA-PPA treatment caused no structural damages to the major organs in HCC mice, indicating low side effects in vivo. Meanwhile, aPD-1@TA-PPA treatment showed no damages on the serum markers of liver and renal functions (figure 7I). These results demonstrated that the combined administration of TA and aPD-1 by nanocarrier achieved a safe and efficient therapeutic effect against HCC. Interestingly, aPD-1@TA-PPA treatment mildly improved the liver function in the orthotopic HCC mice, whereas such a liver-protective effect of aPD-1@TA-PPA was not observed in a classical liver injury model induced by carbon tetrachloride (online supplemental figure S8). Thus, we speculate that the liver protection of our nanodrug is likely to be from its antitumor effects, rather than from the liver-protective effect of the drug itself. Taken together, we provided convincing evidences which indicated the remarkable therapeutic efficacy with minimal side effects of our novel nanodrug (aPD-1@TA-PPA) for HCC immunotherapy.

DISCUSSION

Immunotherapy, particularly the FDA-approved ICB (eg, PD-1 inhibitor), has shown great potential for treating various malignant tumors. Nevertheless, PD-1 inhibitor obtained poor objective response rates (15%–20%) in phase I/II trials and failed to meet the primary end points in phase III trials for patients with HCC, which was primarily attributable to ICB resistance induced by the immunosuppressive TME, as well as to drug discontinuation caused by serious immune-related adverse events.[2–4] Thus, novel anti-HCC strategies that can simultaneously overcome ICB resistance and reduce side effects are urgently needed. Aiming at overcoming the aforementioned dilemma, we develop a novel tumor-targeted nanocarrier for the combined delivery of aPD-1 and TA. We confirmed the formed nanodrug (aPD-1@TA-PPA) achieved a highly effective therapy and minimal side effects in vitro and in orthotopic HCC model.

TA, a selective inhibitor of cyclic guanosine monophosphate-specific PDE5, is a common clinically-used drug worldwide for treating erectile dysfunction and pulmonary hypertension.[18] Encouragingly, recent laboratory and clinical studies reveal that TA can effectively antagonize immunosuppression in malignances including head and neck squamous cell carcinoma and multiple myeloma.[38 39] However, few reports provide direct evidence referring the immune regulatory effect of TA in HCC immunotherapy. One important finding of our study is discovery of the effective intervention of

Figure 6

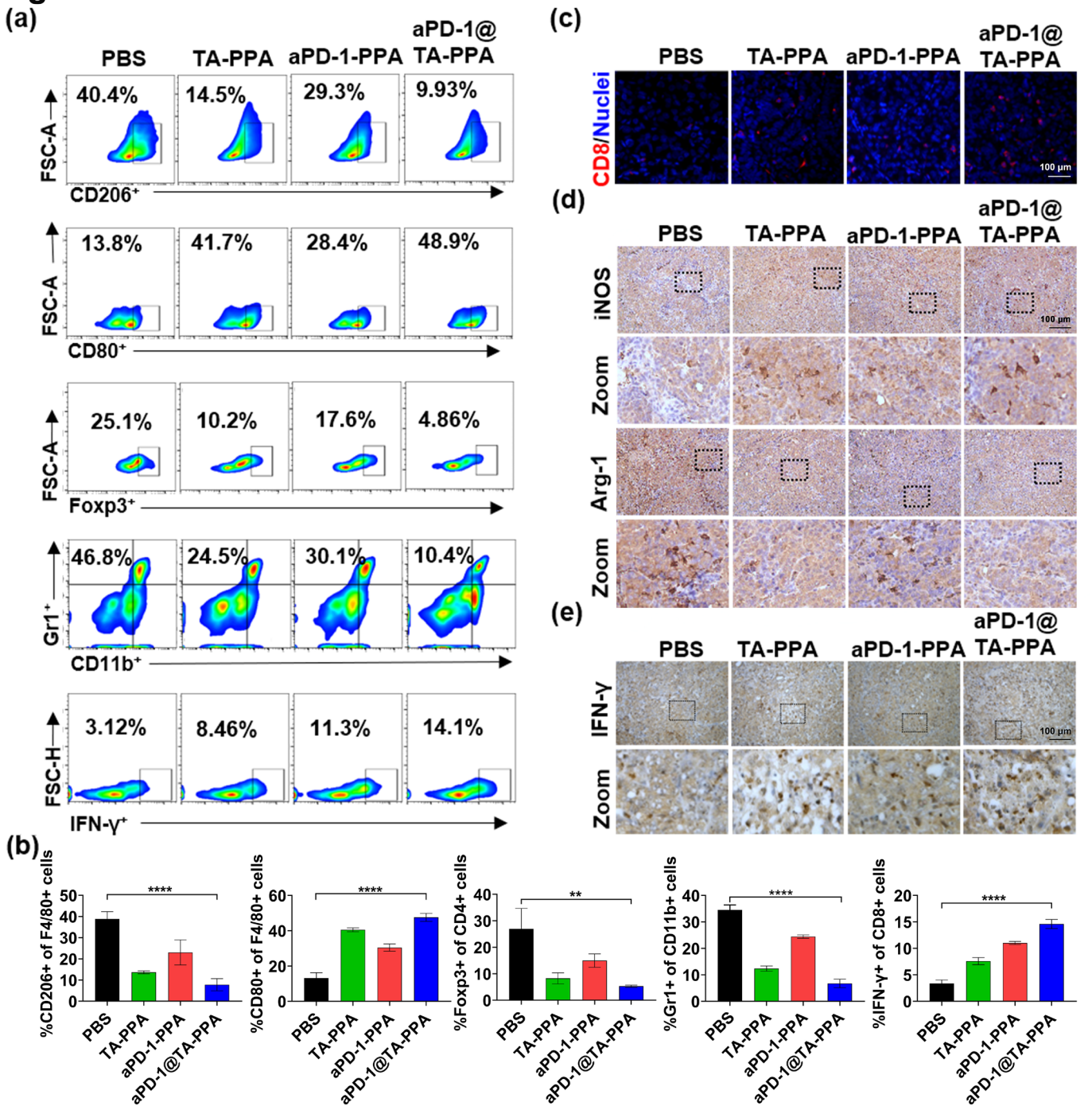

Figure 6 Combined administration of TA and aPD-1 by nanocarrier synergistically regulated TME. (A,B) M1 or M2 TAMs, Tregs, MDSCs and CD8+ T cells in the Hep1-6 tumor tissue from orthotopic HCC mice receiving various treatments were quantitatively determined by flow cytometry assay (n=3). (C) Representative immunofluorescent staining showed CD8+ T cells in Hep1-6 tumor tissues. (D,E) The key markers of M2 TAMs (Arg1) and M1 TAMs (iNOS), as well as the IFN-γ expression levels in Hep1-6 tumor tissues were revealed by immunohistochemical staining. **P<0.01, ****P<0.0001. aPD-1, programmed cell death receptor 1 antibody; HCC, hepatocellular carcinoma; IFN-γ, interferon gamma; MDSC, myeloid-derived suppressor cell; PBS, phosphate-buffered saline; TA, tadalafil; TAM, tumor-associated macrophage; TME, tumor microenvironment.

TA in the metabolism–immunity crosstalk in the TME as evidence by the inhibitory role of TA in M2 polarization and Arg1/polyamine metabolism of TAMs both in vitro and in orthotopic HCC model. It is notorious that tumor cells reprogram their metabolism to adjust to harsh environments. For instance, our previous study demonstrated that heat stress-challenged HCC cells enhanced aerobic glycolysis metabolism to improve their survival ability.[40] Recently, growing research indicate that metabolic reprogramming of the immune cells in TME is vital

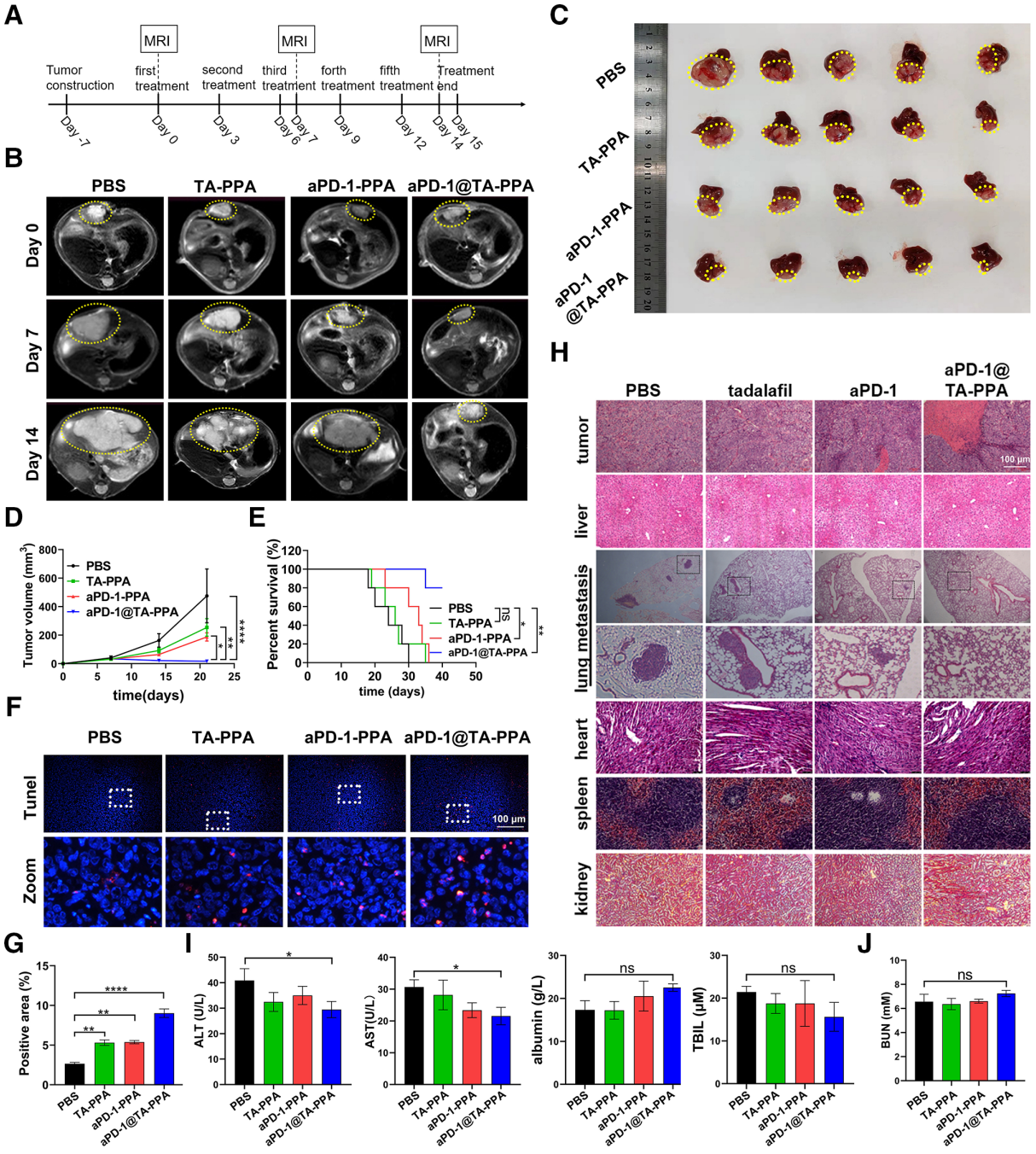

Figure 7 Combined administration of TA and aPD-1 by nanocarrier achieved remarkable therapeutic effect in HCC. (A) Schematic diagram of nanodrug therapy for mice bearing orthotopic Hep1-6 HCC. (B) Monitoring the tumor growth by T2WI at different times. (C) General view of orthotopic HCC in different groups. (D) Tumor growth of the orthotopic HCC measured by MRI scan. n=5. (e) Survival curves of the orthotopic HCC mice. n=5. (F,G) The tumor apoptosis was detected by TUNEL staining. (H) H&E staining of the tumor, lung, heart, spleen, and kidney tissues harvested from different groups. (i) Serum levels of ALT, AST, TBIL, albumin and BUN in mice measured at day 15 (n=3). *P<0.05, **P<0.01, ****P<0.0001. ALT, alanine transaminase; aPD-1, programmed cell death receptor 1 antibody; AST, aspartate aminotransferase; HCC, hepatocellular carcinoma; ns, no significance. BUN, blood urea nitrogen; PBS, phosphate-buffered saline; T2WI, T2-weighted MRI; TA, tadalafil; TBIL, total bilirubin.

for immunosuppression and tumor progression. Particularly, M2 macrophages were found to make use of upregulated Arg1 to convert arginine into polyamine, thus consuming the arginine required for T-cell function and impairing T-cell cytotoxicity.[13 14] Furthermore, the overproduced polyamine not only increases IDO1 expression to mediate the disability of dendritic cells but also induces the apoptosis of T cells and natural killer cells, which collectively contributes to an immunosuppressive TME.[11] After making clear the inhibition of TA on M2 polarization and polyamine production of TAMs, the effective regulation of TA on immunosuppressive TME was

further confirmed by our observations that TA was also capable of inhibiting the immunosuppressive MDSCs and Tregs, and promoting the proimmune, antitumor CD8+ T cells. Noteworthily, the direct action of TA on the proliferation, apoptosis and invasion of tumor cells was excluded (online supplemental figure S9). These results make a good pharmacological explanation for the role of TA in conquering ICB resistance, and for the synergistically improved outcome of the combination therapy of aPD-1@TA-PPA in orthotopic HCC mice.

For a deeper insight into the previously unknown role and mechanisms of TA as antitumor drug candidate for conquering ICB resistance, the dual regulation of M2 TAMs and MDSCs by TA is worthy of attention. MDSCs not only can produce abundant immunosuppressive factors to directly impair T cell cytotoxicity, but also can transdifferentiate into immunosuppressive M2 TAMs to be a constant source for M2 TAMs,[10] which well explains why monotherapy targeting the M2 TAMs or MDSCs alone failed to achieve satisfactory outcomes for conquering ICB resistance.[41 42] Noteworthily, CCL2, a classical chemokine with potent ability of recruiting immunosuppressive cells including MDSCs and Tregs, was significantly reduced by TA treatment in the HCC tissues. Although the mechanism underlying such an effect of TA remains unclear, we speculate that CCL2 might be a vital mediator involved in the regulation of TA on the immunosuppressive TME, which contributes to overcoming ICB resistance and partially accounts for the synergistically enhanced efficacy of the aPD-1@TA-PPA combination therapy for HCC treatment.

Apart from the aforementioned pharmacological mechanism, in further view to the pharmacokinetics aspect, an efficient tumor-targeted delivery of aPD-1 and TA by our workable strategy also plays a crucial role in the improved efficacy of combination therapy. In present study, based on our previous work,[23] we further developed a novel nanodrug (aPD-1@TA-PPA) carrying aPD-1 on its surface and encapsulating hydrophobic TA in its hydrophobic core based on a tailor-made block copolymer with dual pH sensitivities. On one hand, aPD-1@TA-PPA facilitates passive tumor targeting via the enhanced permeability and retention (EPR) effect,[43] a previously well-verified effect through which core-shell structural nanoscale micelles are capable of accumulating in tumor sites. On the other hand, aPD-1@TA-PPA can probably bind to circulating PD-1+ T cells in the blood to realize an unconventional tumor-targeted delivery via tumor recruitment of nanodrug-bound T cells. Noteworthily, growing recent studies have revealed that EPR effect is heterogeneous in humans and even may not exist in some tumors, leading to a much less effective tumor accumulation of nanodrugs.[44] Thus, our T cell-mediated targeted strategy provided a potent supplement to the EPR-driven passive tumor accumulation of the nanodrug. In addition, based on our previous study, making use of dual-sensitive nanocarrier to facilitate highly efficient and targeted drug release in pathological microenvironment,[23] we introduced a tailor-made block copolymer to endow aPD-1@TA-PPA with the property of dual pH-sensitive drug release. In response to the TME weak acidity (pH~6.5), aPD-1@TA-PPA delivered to the tumor tissue by either recruiting nanodrug-bound PD-1+ T cells or EPR effect triggers the first-stage drug release in TME to provide aPD-1 for blocking THE PD-1–PD-1 axis to activate the tumor-killing cytotoxic T cells. Meanwhile, the first-stage drug release also leads to a surface charge reversal from negative to positive, leaving a positively charged TA-encapsulated micelle (TA-PPA) which allows an easier drug internalization into M2 macrophages and MDSCs. Next, in response to the strong acidity of lysosomal microenvironment, TA-PPA triggers the rapid second-stage drug release to provide TA for dually inhibiting M2 macrophages and MDSCs to reverse immunosuppressive TME. Taken together, we offered a nanomedicine strategy for tumor-targeted dual-drug delivery to gain remarkable efficacy with minimal side effects in HCC treatment.

CONCLUSIONS

In current study, aiming at simultaneously overcoming ICB resistance and reducing side effects, we develop a T cell-mediated tumor-targeted nanocarrier for the combined delivery of aPD-1 and TA. We confirmed the formed nanodrug (aPD-1@TA-PPA) achieved a highly effective therapy and minimal side effects in vitro and in orthotopic HCC model. Our novel nanomedicine strategy promotes the clinical translational application of dual-drug combination therapy (eg, ICB and novel immunological adjuvant) for HCC and other refractory tumors.

Author affiliations
[1]Laboratory of Interventional Radiology, Department of Minimally Invasive Interventional Radiology and Interventional Cancer Center, the Second Affiliated Hospital, Guangzhou Medical University, Guangzhou, China
[2]College of Chemistry and Materials Science, Jinan University, Guangzhou, China
[3]PCFM Lab of Ministry of Education School of Materials Science and Engineering, Sun Yat-Sen University, Guangzhou, China

Acknowledgements The authors thank Liang Licong, Tan Yitong, Chen Gengjia, Cai Weiguo, and Guo Zhaoxiong for assistance with the experiment performance.

Contributors KZ, LL, and YW designed and conceived this project. XW, QZ, JZ, and ZX performed experiments and wrote the manuscript. JL, SD, and XH performed the experiments. WH, MC, YG, and JH analyzed and interpreted the data. KZ, LL, YW, WH, MC, and JH acquired fundings. KZ accepts full responsibility for the work and/or the conduct of the study, had access to the data, and controlled the decision to publish.

Funding This work was funded by the National Natural Science Foundation of China (82001929, 82172043, 52173125, and 82001930), the Science and Technology Project of Guangzhou (202002030135, 202102020393, 202102010082, and 202201010633), and the Youth Innovative Talents Project of Guangdong Province University (2020KQNCX057).

Competing interests None declared.

Patient consent for publication Not applicable.

Ethics approval All animal procedures were performed in accordance with the National Institutes of Health Guide for the Care and Use of Laboratory Animals and approved by the ethics committee on the Care and Use of Laboratory Animals in the Second Affiliated Hospital of Guangzhou Medical University (Guangzhou, China; ID number A2019-046).

Provenance and peer review Not commissioned; externally peer reviewed.

Data availability statement Data are available upon reasonable request.

ORCID iD

Kangshun Zhu http://orcid.org/0000-0001-5142-010X

REFERENCES

1 Sung H, Ferlay J, Siegel RL, *et al*. Global cancer statistics 2020: GLOBOCAN estimates of incidence and mortality worldwide for 36 cancers in 185 countries. *CA Cancer J Clin* 2021;71:209–49.
2 Zhu AX, Finn RS, Edeline J, *et al*. Pembrolizumab in patients with advanced hepatocellular carcinoma previously treated with sorafenib (KEYNOTE-224): a non-randomised, open-label phase 2 trial. *Lancet Oncol* 2018;19:940–52.
3 Finn RS, Ryoo B-Y, Merle P, *et al*. Pembrolizumab as second-line therapy in patients with advanced hepatocellular carcinoma in KEYNOTE-240: a randomized, double-blind, phase III trial. *J Clin Oncol* 2020;38:193–202.
4 Lee-Chang C, Miska J, Hou D, *et al*. Activation of 4-1BBL+ B cells with CD40 agonism and IFNγ elicits potent immunity against glioblastoma. *J Exp Med* 2021;218:e20200913.
5 Zhou Z, Lin L, An Y, *et al*. The combination immunotherapy of TLR9 agonist and OX40 agonist via intratumoural injection for hepatocellular carcinoma. *J Hepatocell Carcinoma* 2021;8:529–43.
6 Donelan W, Dominguez-Gutierrez PR, Kusmartsev S. Deregulated hyaluronan metabolism in the tumor microenvironment drives cancer inflammation and tumor-associated immune suppression. *Front Immunol* 2022;13:971278.
7 Wang Y, Johnson KCC, Gatti-Mays ME, *et al*. Emerging strategies in targeting tumor-resident myeloid cells for cancer immunotherapy. *J Hematol Oncol* 2022;15:118.
8 Li D, Zhang Q, Li L, *et al*. B2-Microglobulin maintains glioblastoma stem cells and induces M2-like polarization of tumor-associated macrophages. *Cancer Res* 2022;82:3321–34.
9 Zhang J, Zhou X, Hao H. Macrophage phenotype-switching in cancer. *Eur J Pharmacol* 2022;931:175229.
10 Liu G, Bi Y, Shen B, *et al*. Sirt1 limits the function and fate of myeloid-derived suppressor cells in tumors by orchestrating HIF-1α-dependent glycolysis. *Cancer Res* 2014;74:727–37.
11 Holbert CE, Cullen MT, Casero RA Jr, *et al*. Polyamines in cancer: integrating organismal metabolism and antitumour immunity. *Nat Rev Cancer* 2022;22:467–80.
12 Bae D-H, Lane DJR, Jansson PJ, *et al*. The old and new biochemistry of polyamines. *Biochim Biophys Acta Gen Subj* 2018;1862:2053–68.
13 Novita Sari I, Setiawan T, Seock Kim K, *et al*. Metabolism and function of polyamines in cancer progression. *Cancer Lett* 2021;519:91–104.
14 Orillion A, Damayanti NP, Shen L, *et al*. Dietary protein restriction reprograms tumor-associated macrophages and enhances immunotherapy. *Clin Cancer Res* 2018;24:6383–95.
15 Alexander ET, Mariner K, Donnelly J, *et al*. Polyamine blocking therapy decreases survival of tumor-infiltrating immunosuppressive myeloid cells and enhances the antitumor efficacy of PD-1 blockade. *Mol Cancer Ther* 2020;19:2012–22.
16 Mondanelli G, Bianchi R, Pallotta MT, *et al*. A relay pathway between arginine and tryptophan metabolism confers immunosuppressive properties on dendritic cells. *Immunity* 2017;46:233–44.
17 Hayes CS, Shicora AC, Keough MP, *et al*. Polyamine-blocking therapy reverses immunosuppression in the tumor microenvironment. *Cancer Immunol Res* 2014;2:274–85.
18 Francis SH, Busch JL, Corbin JD, *et al*. Cgmp-Dependent protein kinases and cGMP phosphodiesterases in nitric oxide and cGMP action. *Pharmacol Rev* 2010;62:525–63.
19 Yu SJ, Ma C, Heinrich B, *et al*. Targeting the crosstalk between cytokine-induced killer cells and myeloid-derived suppressor cells in hepatocellular carcinoma. *J Hepatol* 2019;70:449–57.
20 Yamaguchi T, Uenaka K, Imaoka T. Pharmacological, pharmacokinetic, and clinical profile of tadalafil (Cialis). *Nihon Yakurigaku Zasshi* 2008;131:469–77.
21 Sabri MR, Bigdelian H, Hosseinzadeh M, *et al*. Comparison of the therapeutic effects and side effects of tadalafil and sildenafil after surgery in young infants with pulmonary arterial hypertension due to systemic-to-pulmonary shunts. *Cardiol Young* 2017;27:1686–93.
22 Huang B, Abraham WD, Zheng Y, *et al*. Active targeting of chemotherapy to disseminated tumors using nanoparticle-carrying T cells. *Sci Transl Med* 2015;7:291ra94.
23 Xiao Z, Su Z, Han S, *et al*. Dual ph-sensitive nanodrug blocks PD-1 immune checkpoint and uses T cells to deliver NF-κB inhibitor for antitumor immunotherapy. *Sci Adv* 2020;6:eaay7785.
24 Kumari N, Choi SH. Tumor-associated macrophages in cancer: recent advancements in cancer nanoimmunotherapies. *J Exp Clin Cancer Res* 2022;41:68.
25 Liu N, Zhang J, Yin M, *et al*. Inhibition of xct suppresses the efficacy of anti-PD-1/L1 melanoma treatment through exosomal PD-L1-induced macrophage M2 polarization. *Mol Ther* 2021;29:2321–34.
26 Hensler M, Kasikova L, Fiser K, *et al*. M2-Like macrophages dictate clinically relevant immunosuppression in metastatic ovarian cancer. *J Immunother Cancer* 2020;8:e000979.
27 Thakur A, Schalk D, Sarkar SH, *et al*. A Th1 cytokine-enriched microenvironment enhances tumor killing by activated T cells armed with bispecific antibodies and inhibits the development of myeloid-derived suppressor cells. *Cancer Immunol Immunother* 2012;61:497–509.
28 Todorović-Raković N. The role of cytokines in the evolution of cancer: IFN-γ paradigm. *Cytokine* 2022;151.
29 Xiao Z, Cai Y, Wang X, *et al*. Nanodrug simultaneously regulates stromal extracellular matrix and glucose metabolism for effective immunotherapy against orthotopic pancreatic cancer. *Nano Today* 2022;44:101490.
30 Huang J, Zheng C, Xiao H, *et al*. A polymer-calcium phosphate nanocapsule for rnai-induced oxidative stress and cascaded chemotherapy. *J Control Release* 2021;340:259–70.
31 Su Z, Xiao Z, Wang Y, *et al*. Codelivery of anti-PD-1 antibody and paclitaxel with matrix metalloproteinase and pH dual-sensitive micelles for enhanced tumor chemoimmunotherapy. *Small* 2020;16:e1906832.
32 Elbardisy B, Galal S, Abdelmonsif DA, *et al*. Intranasal tadalafil nanoemulsions: formulation, characterization and pharmacodynamic evaluation. *Pharm Dev Technol* 2019;24:1083–94.
33 Kong D, Jiang Y, Miao X, *et al*. Tadalafil enhances the therapeutic efficacy of BET inhibitors in hepatocellular carcinoma through activating hippo pathway. *Biochim Biophys Acta Mol Basis Dis* 2021;1867:166267.
34 Dai Y, Xu C, Sun X, *et al*. Nanoparticle design strategies for enhanced anticancer therapy by exploiting the tumour microenvironment. *Chem Soc Rev* 2017;46:3830–52.
35 Cheng A-L, Hsu C, Chan SL, *et al*. Challenges of combination therapy with immune checkpoint inhibitors for hepatocellular carcinoma. *J Hepatol* 2020;72:307–19.
36 Xu M, Wang Y, Xia R, *et al*. Role of the CCL2-CCR2 signalling axis in cancer: mechanisms and therapeutic targeting. *Cell Prolif* 2021;54:e13115.
37 Peña-Asensio J, Calvo H, Torralba M, *et al*. Anti-Pd-1/Pd-L1 based combination immunotherapy to boost antigen-specific CD8+ T cell response in hepatocellular carcinoma. *Cancers (Basel)* 2021;13:1922.
38 Luginbuhl AJ, Johnson JM, Harshyne LA, *et al*. Tadalafil enhances immune signatures in response to neoadjuvant nivolumab in resectable head and neck squamous cell carcinoma. *Clin Cancer Res* 2022;28:915–27.
39 Noonan KA, Ghosh N, Rudraraju L, *et al*. Targeting immune suppression with PDE5 inhibition in end-stage multiple myeloma. *Cancer Immunol Res* 2014;2:725–31.
40 Chen Y, Bei J, Liu M, *et al*. Sublethal heat stress-induced O-glcnacylation coordinates the warburg effect to promote hepatocellular carcinoma recurrence and metastasis after thermal ablation. *Cancer Lett* 2021;518:23–34.
41 Ma Z, Yang M, Foda MF, *et al*. Polarization of tumor-associated macrophages promoted by vitamin C-loaded liposomes for cancer immunotherapy. *ACS Nano* 2022;16:17389–401.
42 Li R, Salehi-Rad R, Crosson W, *et al*. Inhibition of granulocytic myeloid-derived suppressor cells overcomes resistance to immune

checkpoint inhibition in LKB1-deficient non-small cell lung cancer. *Cancer Res* 2021;81:3295–308.
43 Kalyane D, Raval N, Maheshwari R, *et al*. Employment of enhanced permeability and retention effect (EPR): nanoparticle-based precision tools for targeting of therapeutic and diagnostic agent in cancer. *Mater Sci Eng C Mater Biol Appl* 2019;98:1252–76.
44 Danhier F. To exploit the tumor microenvironment: since the EPR effect fails in the clinic, what is the future of nanomedicine? *J Control Release* 2016;244:108–21.